Measuring the galaxy power spectrum with multiresolution decomposition – IV. redshift distortion

XiaoHu Yang[1,2] Long-Long Feng[1,2,3] YaoQuan Chu[1,2] Li-Zhi Fang[4]

Received ____________________; accepted ____________________

[1]Center for Astrophysics, University of Science and Technology of China, Hefei, Anhui 230026,P.R.China

[2]National Astronomical Observatories, Chinese Academy of Science, Chao-Yang District, Beijing, 100012, P.R. China

[3]Institute for Theoretical Physics, Academic of Science, Beijing, 100080, P.R. China

[4]Department of Physics, University of Arizona, Tucson, AZ 85721

ABSTRACT

In this paper, we develop a theory of redshift distortion of the galaxy power spectrum in the discrete wavelet transform (DWT) representation. Because the DWT power spectrum is dependent of both the scale and shape (configuration) of the decomposition modes, it is sensitive to distortion of shape of the field. On the other hand, the redshift distortion causes a shape distortion of distributions in real space with respect to redshift space. Therefore, the shape-dependent DWT power spectrum is useful to detect the effect of redshift distortion. We first established the mapping between the DWT power spectra in redshift and real space. The mapping depends on the redshift distortion effects of (1) bulk velocity, (2) selection function and (3) pairwise peculiar velocity. We then proposed β-estimators using the DWT off-diagonal power spectra. These β-estimators are model-free even when the non-linear redshift distortion effect is not negligible. Moreover, these estimators do not rely on the assumption of whether the pairwise velocity dispersion being scale-dependent. The tests with N-body simulation samples show that the proposed β-estimators can yield reliable measurements of β with about 20% uncertainty for all popular dark matter models. We also develop an algorithm for reconstruction of the power spectrum in real space from the redshift distorted power spectrum. The numerical test also shows that the real power spectrum can be well recovered from the redshift distorted power spectrum.

Subject headings: cosmology: theory - large-scale structure of universe

1. Introduction

In three previous papers we have developed a method of measuring galaxy power spectrum with discrete wavelet transform (DWT) decomposition, which is an alternative of the Fourier power spectrum detection (Fang & Feng, 2000 (paper I), Yang et al 2001a (paper II), 2001b (paper III)). The DWT power spectrum estimator is information-loseless, and optimized in the sense that the spatial resolution is adaptive automatically to the scale to be studied. A test with observed sample of the LCRS galaxies showed that the DWT estimator can give a robust measurement of the power spectrum.

In this paper, we continue our effort in this direction. The topic this time is to develop theory and algorithm of redshift distortion in the DWT representation.

In terms of power spectrum measurement, the central problem of redshift distortion is to find the mapping between the power spectra in redshift and physical spaces. In our paper II, we have already studied this mapping. However, that mapping is directly obtained by a wavelet transform of the mapping of the power spectrum in the Fourier representation (Peacock & Dodds 1994). Although a Fourier mode can be transformed into DWT modes and *vice versa*, we should be careful in doing the transform of a second order statistical quantity from the Fourier representation into the DWT one. As we have showed in paper I, the covariance of density contrast in the DWT representation $\langle \epsilon_{\mathbf{j},\mathbf{l}} \epsilon_{\mathbf{j}',\mathbf{l}'} \rangle$ is not equivalent to the Fourier counterpart $\langle \hat{\delta}_{\mathbf{k}} \hat{\delta}_{\mathbf{k}} \rangle$, because the Fourier mode is subjected to the central limit theorem, while mode localized in both scale and physical space may not be so. This is because the DWT mode is characterized by not only the scale, but also the configuration (or shape) of the mode. Simply speaking, the variance $\langle \epsilon_{\mathbf{j},\mathbf{l}} \epsilon_{\mathbf{j}',\mathbf{l}'} \rangle$ contains information of both the scale and phase (shape), while $\langle \hat{\delta}_{\mathbf{k}} \hat{\delta}_{\mathbf{k}} \rangle$ does not contain information of phases (Fang & Thews 1998).

We have found in paper II that, the Fourier mapping of redshift distortion can be

employed for diagonal DWT power spectrum, but not off-diagonal DWT power spectrum. This is due to the shape(phase)-dependence of DWT modes. A 3-D Fourier mode with wave-vector $\mathbf{k} = (k_1, k_2, k_3)$ can be transformed into mode $\mathbf{k}' = (k'_1, k'_2, k'_3)$ by a coordinate rotation as long as $k_1^2 + k_2^2 + k_3^2 = k_1'^2 + k_2'^2 + k_3'^2$. Therefore, for an isotropic random field, the Fourier modes with the same $k = |\mathbf{k}|$ are statistically equivalent. However, the DWT modes do not share the same property. The length scale of a 3-D wavelet mode with scale index $\mathbf{j} = (j_1, j_2, j_3)$ is $L/[2^{2j_1} + 2^{2j_2} + 2^{2j_3}]^{1/2}$, where L is the length scale of the sample. Generally, one cannot transform a mode (j_1, j_2, j_3) to (j'_1, j'_2, j'_3) by a rotation, even if they have the same scale.

As a consequence, the redshift distortion in the DWT presentation will be shape-dependent. For instance, in the Fourier representation, the linear redshift distortion factor $(1 + \beta\mu^2)^2$ (Kaiser 1987), where β is the so-called redshift distortion parameter, depends only on $\mu = k_3/k$, i.e. the cosine of the angle between the wavevector $\mathbf{k}$ and the line-of-sight. While in the DWT representation, the linear redshift distortion factor will depend on not only the scale, but also the shape of DWT modes.

An important application of redshift distortion is to determine the redshift distortion parameter β (e.g. Hamilton 1998), which contains valuable information of the cosmological mass density parameter and the bias of galaxies. The shape-dependence of redshift distortion is very useful for the parameter determination. We will develop an algorithm of β estimation with diagonal and off-diagonal DWT power spectra.

Moreover, the DWT representation provides an easy way to study the effect of selection function on the redshift distortion. In the first three papers, we assumed that the selection function $\bar{n}(\mathbf{x})$ is known. Actually, the "known" is not necessary. According to the definition, selection function is an observed galaxy distribution if galaxy clustering is absent. Therefore, for a consistent algorithm of power spectrum, the selection function

should be and can be obtained by the galaxy distribution itself. We will show that in the DWT representation the selection function can be determined by the distribution of galaxies without other assumption. This algorithm is convenient to estimate the contribution of selection function to redshift distortion.

The paper will be organized as follows. §2 is a summary of the algorithm of the DWT power spectrum. In §3, we develop a theory of the redshift distortion with a multiresolution analysis. The emphases are the real-redshift mapping of diagonal and off-diagonal power spectrum. We proposed β-estimators, which are tested by N-body simulation samples of popular dark matter models (§4 and 5). Finally, the conclusions and discussions will be presented in §6. The mathematical stuffs with the relevant DWT quantities are given in Appendix.

2. Algorithm of the DWT power spectrum

2.1. The DWT power spectrum

We summarize the algorithm of the DWT power spectrum. The details can be found in Fang & Feng (2000) and Yang et al (2001).

If the position measurement is perfectly precise, the number density distribution of galaxies can be written as

$$n^g(\mathbf{x}) = \sum_{i=1}^{N_g} w_i \delta_D(\mathbf{x} - \mathbf{x}_i) = \bar{n}(\mathbf{x})[1 + \delta(\mathbf{x})] \tag{1}$$

where N_g is the total number of galaxies, $\mathbf{x_i}$ is position of ith galaxy, w_i is its weight, and δ_D the 3-D Dirac δ function. $\bar{n}(\mathbf{x})$ is selection function given by the mean number density of galaxies when galaxy clustering is absent, and $\delta(\mathbf{x})$ is the density contrast fluctuation in the underlying matter distribution.

Without loss of generality, we enclose the sample in a cubic box with side lengths (L_1, L_2, L_3). In the DWT representation, $n^g(\mathbf{x})$ is decomposed into

$$n^g(\mathbf{x}) = n^{(\mathbf{j})}(\mathbf{x}) + \sum_{n=1}^{7} \sum_{j'_1=j_1}^{\infty} \sum_{j'_2=j_2}^{\infty} \sum_{j'_3=j_3}^{\infty} \sum_{l_1=0}^{2^{j'_1}-1} \sum_{l_2=0}^{2^{j'_2}-1} \sum_{l_3=0}^{2^{j'_3}-1} \tilde{\epsilon}^{g,n}_{\mathbf{j}',\mathbf{l}} \psi^{(n)}_{\mathbf{j}',\mathbf{l}}(\mathbf{x}), \tag{2}$$

where, $n^{(\mathbf{j})}(\mathbf{x})$ is given by

$$n^{(\mathbf{j})}(\mathbf{x}) = \sum_{l_1=0}^{2^{j_1}-1} \sum_{l_2=0}^{2^{j_2}-1} \sum_{l_3=0}^{2^{j_3}-1} \epsilon^g_{\mathbf{j},\mathbf{l}} \phi_{\mathbf{j},\mathbf{l}}(\mathbf{x}). \tag{3}$$

The index $\mathbf{j} = (j_1, j_2, j_3)$ stand for 3-D scales $L_2/2^{j_1}, L_2/2^{j_2}, L_3/2^{j_3}$, and index $\mathbf{l} = (l_1, l_2, l_3)$ for the position of cell $l_1 L_1/2^{j_1} < x_1 \leq (l_1+1)L_1/2^{j_1}$, $l_2 L_2/2^{j_2} < x_2 \leq (l_2+1)L_2/2^{j_2}$, $l_3 L_3/2^{j_3} < x_3 \leq (l_3+1)L_3/2^{j_3}$.

In eq.(3), $\epsilon^g_{\mathbf{j},\mathbf{l}}$ is called scaling function coefficient (SFC) of $n^g(\mathbf{x})$. They are given by

$$\epsilon^g_{\mathbf{j},\mathbf{l}} = \int n^g(\mathbf{x}) \phi_{\mathbf{j},\mathbf{l}}(\mathbf{x}) d\mathbf{x} = \sum_{i=1}^{N_g} w_i \phi_{\mathbf{j},\mathbf{l}}(\mathbf{x}_i), \tag{4}$$

where we have used equation (1) in the last step. The scaling functions $\phi_{\mathbf{j},\mathbf{l}}(\mathbf{x})$ play the role of window functions for the cell with volume $(L_1/2^{j_1}) \times (L_2/2^{j_2}) \times (L_3/2^{j_3})$, and located at position $\mathbf{l}$. Therefore, the SFC $\epsilon^g_{\mathbf{j},\mathbf{l}}$ is the mean of field $n^g(\mathbf{x})$ in the volume $(L_1/2^{j_1}) \times (L_2/2^{j_2}) \times (L_3/2^{j_3})$ at position $\mathbf{l}$. Thus, the term $n^{(\mathbf{j})}(\mathbf{x})$ of eqs.(2) and (3) actually is the smoothed $n^{(\mathbf{j})}(\mathbf{x})$ by window on scale $\mathbf{j}$.

The 3-D scaling functions $\phi_{\mathbf{j},\mathbf{l}}(\mathbf{x})$ can be constructed by a direct product of 1-D scaling functions, i.e.

$$\phi_{\mathbf{j},\mathbf{l}}(\mathbf{x}) = \phi_{j_1,l_1}(x_1)\phi_{j_2,l_2}(x_2)\phi_{j_3,l_3}(x_3). \tag{5}$$

In eq.(2), $\psi^{(n)}_{\mathbf{j},\mathbf{l}}(\mathbf{x})$ are wavelets. An 1-D wavelet $\psi_{j,l}(x)$ is the modes used to extract the fluctuations of a 1-D field $n(x)$ on scale $L/2^j$ at position $\mathbf{l}$. The 3-D wavelets $\psi^{(n)}_{\mathbf{j},\mathbf{l}}(\mathbf{x})$ are given by mixed direct products of 1-D scaling functions $\phi_{j,l}(x)$ and wavelets $\psi_{j,l}(x)$ as

follows,

$$
\begin{aligned}
\psi^{(1)}_{\mathbf{j}',\mathbf{l}}(\mathbf{x}) &= \phi_{j'_1,l_1}(x_1)\phi_{j'_2,l_2}(x_2)\psi_{j'_3,l_3}(x_3)\delta_{j'_1,j_1}\delta_{j'_2,j_2} \\
\psi^{(2)}_{\mathbf{j}',\mathbf{l}}(\mathbf{x}) &= \phi_{j'_1,l_1}(x_1)\psi_{j'_2,l_2}(x_2)\phi_{j'_3,l_3}(x_3)\delta_{j'_1,j_1}\delta_{j'_3,j_3} \\
\psi^{(3)}_{\mathbf{j}',\mathbf{l}}(\mathbf{x}) &= \psi_{j'_1,l_1}(x_1)\phi_{j'_2,l_2}(x_2)\phi_{j'_3,l_3}(x_3)\delta_{j'_2,j_2}\delta_{j'_3,j_3} \\
\psi^{(4)}_{\mathbf{j}',\mathbf{l}}(\mathbf{x}) &= \phi_{j'_1,l_1}(x_1)\psi_{j'_2,l_2}(x_2)\psi_{j'_3,l_3}(x_3)\delta_{j'_1,j_1} \\
\psi^{(5)}_{\mathbf{j}',\mathbf{l}}(\mathbf{x}) &= \psi_{j'_1,l_1}(x_1)\phi_{j'_2,l_2}(x_2)\psi_{j'_3,l_3}(x_3)\delta_{j'_2,j_2} \\
\psi^{(6)}_{\mathbf{j}',\mathbf{l}}(\mathbf{x}) &= \psi_{j'_1,l_1}(x_1)\psi_{j'_2,l_2}(x_2)\phi_{j'_3,l_3}(x_3)\delta_{j'_3,j_3} \\
\psi^{(7)}_{\mathbf{j}',\mathbf{l}}(\mathbf{x}) &= \psi_{j'_1,l_1}(x_1)\psi_{j'_2,l_2}(x_2)\psi_{j'_3,l_3}(x_3).
\end{aligned}
\tag{6}
$$

Accordingly, $\psi^{(n)}_{\mathbf{j}',\mathbf{l}}(\mathbf{x})$ with $n = 1, 2, 3$ describe 2-D projected fluctuations on a slice, and $n = 4, 5, 6$ 1-D fluctuations along a line. $\psi^{(7)}_{\mathbf{j}',\mathbf{l}}(\mathbf{x})$ describes the 3-D fluctuations inside the cell $\mathbf{l} = (l_1, l_2, l_3)$ on a scale j'.

Hereafter, we consider the projection of density fluctuations onto the space spanned by $\psi^{(7)}_{\mathbf{j}',\mathbf{l}}(\mathbf{x})$ only. For simplicity, we ignore the upper index $n = 7$ in the notations of $\psi^{(n)}_{\mathbf{j}',\mathbf{l}}(\mathbf{x})$ and $\tilde{\epsilon}^{g,n}_{\mathbf{j}',\mathbf{l}}$ without confusion. Thus, the wavelet function coefficient (WFC) $\tilde{\epsilon}^{g}_{\mathbf{j},\mathbf{l}}$ of $n^g(\mathbf{x})$ is given by

$$
\tilde{\epsilon}^{g}_{\mathbf{j},\mathbf{l}} = \int n^g(\mathbf{x})\psi_{\mathbf{j},\mathbf{l}}(\mathbf{x})d\mathbf{x} = \sum_{i=1}^{N_g} w_i \psi_{\mathbf{j},\mathbf{l}}(\mathbf{x}_i),
\tag{7}
$$

Therefore, the WFC $\tilde{\epsilon}^{g}_{\mathbf{j},\mathbf{l}}$ is the amplitude of the fluctuations of the field $n^g(\mathbf{x})$ on scale $(L_1/2^{j_1}) \times (L_2/2^{j_2}) \times (L_3/2^{j_3})$ at position $\mathbf{l}$.

The functions $\phi_{\mathbf{j},\mathbf{l}}(\mathbf{x})$ and $\psi^{(n)}_{\mathbf{j},\mathbf{l}}(\mathbf{x})$ form a complete and orthonormal basis in space of functions defined in 3-dimensional coordinate space. The decomposition of eq.(2) is information loseless.

The DWT power spectrum of $\delta(\mathbf{x})$ can be estimated by

$$
P_{\mathbf{j}} = \left\langle \frac{[\tilde{\epsilon}^{g}_{\mathbf{j},\mathbf{l}}]^2}{n^2(\mathbf{j},\mathbf{l})} \right\rangle - \left\langle \frac{1}{n(\mathbf{j},\mathbf{l})} \right\rangle,
\tag{8}
$$

where $\langle ... \rangle$ is the average over ensemble. The first term on the r.h.s. is the normalized power from $n^g(\mathbf{x})$, and the second term corrects for the Poisson noise. The normalization factor $n(\mathbf{j}, \mathbf{l})$ is the mean selection function in the mode $(\mathbf{j}, \mathbf{l})$, i.e., the number density of galaxies in the mode $(\mathbf{j}, \mathbf{l})$ when galaxy clustering is absent. As has been shown in paper I (Fang & Feng 2000), the factor $n(\mathbf{j}, \mathbf{l})$ can be absorbed into the weight factor by

$$\frac{n^g(\mathbf{x})}{\bar{n}(\mathbf{x})} = \sum_{i=1}^{N_g} \frac{1}{\bar{n}(\mathbf{x}_i)} w_i \delta_D(\mathbf{x} - \mathbf{x}_i). \tag{9}$$

Thus, equation(8) yields

$$P_{\mathbf{j}} = \frac{1}{2^{j_1+j_2+j_3}} \sum_{l_1=0}^{2^{j_1}-1} \sum_{l_2=0}^{2^{j_2}-1} \sum_{l_3=0}^{2^{j_3}-1} [\tilde{\epsilon}_{\mathbf{j},\mathbf{l}}]^2 - \frac{1}{2^{j_1+j_2+j_3}} \sum_{l_1=0}^{2^{j_1}-1} \sum_{l_2=0}^{2^{j_2}-1} \sum_{l_3=0}^{2^{j_3}-1} \int \frac{\psi^2_{\mathbf{j},\mathbf{l}}(\mathbf{x})}{\bar{n}(\mathbf{x})} d\mathbf{x}, \tag{10}$$

where the WFC $\tilde{\epsilon}_{\mathbf{j},\mathbf{l}}$ is defined as

$$\tilde{\epsilon}_{\mathbf{j},\mathbf{l}} = \int \frac{n^g(\mathbf{x})}{\bar{n}(\mathbf{x})} \psi_{\mathbf{j},\mathbf{l}}(\mathbf{x}) d\mathbf{x} = \sum_{i=1}^{N_g} \frac{1}{\bar{n}(\mathbf{x}_i)} w_i \psi_{\mathbf{j},\mathbf{l}}(\mathbf{x}_i) \tag{11}$$

2.2. Selection function in the DWT representation

By definition eq.(1), selection function $\bar{n}(\mathbf{x})$ is an observed galaxy distribution if galaxy clustering $\delta(\mathbf{x})$ is absent. That is, equation (1) requires to decompose an observed distribution $n^g(\mathbf{x})$ into two parts: the "background" $\bar{n}(\mathbf{x})$, and the fluctuations $\delta(\mathbf{x})$ upon the background.

This decomposition is not easy if the selection function $\bar{n}(\mathbf{x})$ is position-dependent, i.e. it will mix with the fluctuations to be detected. With the DWT analysis, one is capable of performing this decomposition by a scale-by-scale analysis.

When we study the fluctuations on a scale $\mathbf{j}$, all $\mathbf{x}$-dependencies of $n^g(\mathbf{x})$ on scales larger than this scale play the role as a background. Thus, in terms of the scale $\mathbf{j}$, the background is given by a smooth of $n^g(\mathbf{x})$ on the scale $\mathbf{j}$, i.e. it does not contain information of fluctuations on scales equal to or less than $\mathbf{j}$.

This background has already be found from equations (2) and (3). Because of the orthogonal relation

$$\int \phi_{\mathbf{j},\mathbf{l}}(\mathbf{x})\psi_{\mathbf{j}',\mathbf{l}'}(\mathbf{x})d\mathbf{x} = 0, \quad \text{if one of } j'_i \ (i = 1, 2, 3) \text{ satisfies } \ j'_i \geq j_i, \tag{12}$$

the function $n^{(\mathbf{j})}(\mathbf{x})$ does not contain any information of fluctuations of modes $(\mathbf{j}', \mathbf{l})$ with $j'_i \geq j_i$. Thus, to detect the fluctuation power on the scale $\mathbf{j}$, the function $n^{(\mathbf{j})}(\mathbf{x})$ is recognized as a background field. One can identify the selection function as $n^{(\mathbf{j})}(\mathbf{x})$, i.e.

$$\bar{n}^{(\mathbf{j})}(\mathbf{x}) = \sum_{l_1=0}^{2^{j_1}-1} \sum_{l_2=0}^{2^{j_2}-1} \sum_{l_3=0}^{2^{j_3}-1} \epsilon^g_{\mathbf{j},\mathbf{l}} \phi_{\mathbf{j},\mathbf{l}}(\mathbf{x}), \tag{13}$$

where the superscript $\mathbf{j}$ means that this "selection function" is only for the scale $\mathbf{j}$.

In the plane parallel approximation, selection function depends on x_3 only, i.e. the coordinate in redshift direction. From equation (13), the selection function is given by

$$\bar{n}(x_3) = n^{(00j_3)}(x_3) = \sum_{l_3=0}^{2^{j_3}-1} \epsilon^g_{00j,l} \phi_{j_3,l}(x_3). \tag{14}$$

From equation (6), the SFC $\epsilon^g_{00j,l}$ is actually given by an average of $n^g(\mathbf{x})$ over the plane (x_1, x_2), and decomposition along x_3 direction.

Using equation (14), the WFC $\tilde{\epsilon}_{\mathbf{j},\mathbf{l}}$ is now calculated by

$$\tilde{\epsilon}_{\mathbf{j},\mathbf{l}} = \sum_{i=1}^{N_g} \frac{1}{n^{(00j_3)}(x_{3i})} w_i \psi_{\mathbf{j},\mathbf{l}}(\mathbf{x}_i). \tag{15}$$

which presents a simple algorithm for deriving the selection function from observed galaxy samples.

To test this algorithm, we produce mock galaxy samples using N-body simulation, of which the details will be given in §4. For simplicity, the selection effect is applied along one axis (e.g., x_3 direction) of 3-dimensional Cartesian coordinates under the plane parallel approximation. For the simulation sample in the cubic box with a side length of 256 h^{-1}

Mpc, we replicate the sample along x_3 direction, and choose the mock galaxies located between 100-356 h^{-1} Mpc. A selection function is given by

$$\bar{n}(\mathbf{x}) = \frac{1}{1 + a(x_3/L)^b}, \tag{16}$$

where L is the size of the sample. To be comparable with, for example, the LCRS selection function, the parameters are adopted to be $L = 500$ h^{-1} Mpc, $a = 30$ and $b = 3$.

Fig. 1 displays the DWT diagonal power spectrum P_{jjj} of particle distributions for three typical models with the selection function eq.(14), in which we take $j_3 = 7$. It shows that the power spectrum estimator eqs.(10) and (15) can perfectly recover the DWT power spectrum regardless the selection functions (16). This result will keep unchanged if $j_3 \geq 7$. It means that $n^{00j_3}(\mathbf{x_3})$ gives a proper estimation of selection function if j_3 is high enough. Practically, one can find a properly recovered power spectrum by checking whether it is insensitive to j_3.

It should be pointed out that with the developed algorithm the power spectrum eq.(8) is normalized scale-by-scale. The fluctuation amplitudes $\tilde{\epsilon}^g_{\mathbf{j},\mathbf{l}}$ (WFCs) on scale $\mathbf{j}$ is normalized by $n(\mathbf{j},\mathbf{l})$ or $n^{(0,0,j_3)}(x_3)$ [eq.(15)], which contains fluctuations on all scales larger than $\mathbf{j}$. Therefore, the normalization factor generally is scale-dependent. This is different from conventional normalization, which is scale-independent.

If the field is Gaussian, there is no correlation between $\tilde{\epsilon}^g_{\mathbf{j},\mathbf{l}}$ and $n(\mathbf{j},\mathbf{l})$ or $n^{(0,0,j_3)}(x_3)$. Eq.(8) yields

$$P_j = \left\langle \frac{1}{n^2(\mathbf{j},\mathbf{l})} \right\rangle \left\langle [\tilde{\epsilon}^g_{\mathbf{j},\mathbf{l}}]^2 \right\rangle - \left\langle \frac{1}{n(\mathbf{j},\mathbf{l})} \right\rangle. \tag{17}$$

It has been shown with the so-called "partition of unity" of wavelets that $\langle 1/n^2(\mathbf{j},\mathbf{l})\rangle$ is approximately independent of $\mathbf{j}$. In this case, the power spectrum eq.(8) is the same as that given by conventional normalization (Jamkhedkar, Bi & Fang 2001).

However, for non-Gaussian field, especially, if the perturbations on different scales

are correlated, the small scale fluctuations given by the WFC $\tilde{\epsilon}^g_{\mathbf{j},\mathbf{l}}$ generally are correlated with large scale fluctuation contained in $n(\mathbf{j},\mathbf{l})$ or $n^{(0,0,j_3)}(x_3)$. In this case, the power spectrum eq.(8) is very different from usual power spectrum which doesn't not sensitive to the correlation between perturbations on different scales.

The power spectrum defined by eq.(8) will benefit to calculate the effect of selection function upon the redshift distortion (§3.3).

3. Redshift distortion in the DWT representation

3.1. Velocity field

The redshift distortion is due to peculiar motion of galaxies. For a given mass field $\delta(\mathbf{x})$, the galaxy velocity $\mathbf{v}(\mathbf{x})$ is a random field with mean

$$\mathbf{V}(\mathbf{x}) = \langle \mathbf{v}(\mathbf{x}) \rangle_v, \tag{18}$$

where $\langle .. \rangle_v$ denotes ensemble average for velocity fields. $\mathbf{V}(\mathbf{x})$ is the bulk velocity at $\mathbf{x}$.

In linear regime, the bulk velocity is related to the density contrast by

$$\delta(\mathbf{x}) = -\frac{1}{H_0 \beta} \nabla \cdot \mathbf{V}(\mathbf{x}), \tag{19}$$

where $\beta \simeq \Omega_0^{0.6}/b$ is the redshift distortion parameter at present, i.e. redshift $z \simeq 0$.

The *rms* deviation of velocity $\mathbf{v}(\mathbf{x})$ from the bulk velocity $\mathbf{V}(\mathbf{x})$ is

$$\langle [v_i(\mathbf{x}) - V_i(\mathbf{x})]^2 \rangle_v = \sigma^2_{pv}(\mathbf{x}). \tag{20}$$

In the DWT representation, one can calculate $\sigma^2_{pv}(\mathbf{x})$ by the variance of the WFCs of velocity field, i.e. $\tilde{\epsilon}^v_{\mathbf{j},\mathbf{l}} = \int \mathbf{v}(\mathbf{x}) \psi_{\mathbf{j},\mathbf{l}}(\mathbf{x}) d\mathbf{x}$, which is actually the DWT pairwise peculiar velocity (paper III).

In the paper III, we analyzed the PVD of the velocity fields given by the N-body simulation for the CDM family of models. On large scales, the velocity field is basically gaussian. It is completely described by its mean $\mathbf{V}(\mathbf{x})$ and variance $\sigma_{pv}(\mathbf{x})$. On small scales, the velocity field is significantly non-gaussian. The one point function of $\tilde{\epsilon}^v_{\mathbf{j},\mathbf{l}}$ is lognormal. The two-point pairwise velocity correlation functions are non-zero on scales ≤ 1 h^{-1} Mpc. Moreover, on these scales, the pairwise velocities are also correlated significantly with density fluctuations.

3.2. The DWT power spectrum in redshift space

The position of galaxy i in redshift space is given by $\mathbf{s_i} = \mathbf{x_i} + \hat{\mathbf{r}} v_r(\mathbf{x_i})/H_0$, where v_r is the radial component of $\mathbf{v}(\mathbf{x})$. The number density distribution in redshift space is then

$$n^S(\mathbf{s}) = \sum_{i=1}^{N_g} w_i \delta_D[\mathbf{s} - \mathbf{x}_i - \hat{\mathbf{r}} v_r(\mathbf{x}_i)/H_0] = \bar{n}^S(\mathbf{s})[1 + \delta^S(\mathbf{s})], \tag{21}$$

where $\bar{n}^S(\mathbf{s})$ is the selection function in redshift space. Similar to equation (8), the power spectrum in redshift space is

$$P^S_{\mathbf{j}} = \frac{1}{2^{j_1+j_2+j_3}} \sum_{l_1=0}^{2^{j_1}-1} \sum_{l_2=0}^{2^{j_2}-1} \sum_{l_3=0}^{2^{j_3}-1} [\tilde{\epsilon}^S_{\mathbf{j},\mathbf{l}}]^2 - \frac{1}{2^{j_1+j_2+j_3}} \sum_{l_1=0}^{2^{j_1}-1} \sum_{l_2=0}^{2^{j_2}-1} \sum_{l_3=0}^{2^{j_3}-1} \int \frac{\psi^2_{\mathbf{j},\mathbf{l}}(\mathbf{x})}{\bar{n}^S(\mathbf{x})} d\mathbf{x}, \tag{22}$$

where

$$\tilde{\epsilon}^S_{\mathbf{j},\mathbf{l}} = \int \frac{n^S(\mathbf{s})}{\bar{n}^S(\mathbf{s})} \psi_{\mathbf{j},\mathbf{l}}(\mathbf{s}) d\mathbf{s}. \tag{23}$$

The selection function $\bar{n}^S(\mathbf{s})$ can be determined from the observed distribution $n^S(\mathbf{s})$ by equation (13) or (14). It can then be absorbed into the weight w_i as equation (11) or (15). The effect of the difference between $n^S(\mathbf{s})$ and $n(\mathbf{s})$ will be studied in next section. In this section, we will ignored this effect. Thus, using an auxiliary vector $\mathbf{J}$, equations (21) and (23) yield

$$\tilde{\epsilon}^S_{\mathbf{j},\mathbf{l}} = \sum_{i=1}^{N_g} w_i \int d\mathbf{s}\, \delta_D\left(\mathbf{s} - \mathbf{x}_i + i\nabla_J\right) e^{i\mathbf{J}\cdot\hat{\mathbf{r}} v_r(\mathbf{x}_i)/H_0} \psi_{\mathbf{j},\mathbf{l}}(\mathbf{s})\Big|_{\mathbf{J}=0}, \tag{24}$$

where ∇_J is gradient operator on $\mathbf{J}$.

Subjecting equation (24) to an average over ensemble of velocity, if the velocity field is *gaussian*, we have

$$\begin{aligned}
\langle \tilde{\epsilon}^S_{\mathbf{j},\mathbf{l}} \rangle_v &= \sum_{i=1}^{N_g} w_i \int d\mathbf{s}\, \delta_D\left(\mathbf{s} - \mathbf{x}_i + i\nabla_J\right) \langle e^{i\mathbf{J}\cdot\hat{\mathbf{r}}v_r(\mathbf{x}_i)/H_0} \rangle_v \psi_{\mathbf{j},\mathbf{l}}(\mathbf{s})\Big|_{\mathbf{J}=0} \qquad (25)\\
&= \sum_{i=1}^{N_g} w_i \int d\mathbf{s}\, \delta_D\left(\mathbf{s} - \mathbf{x}_i + i\nabla_J\right) e^{i\mathbf{J}\cdot\hat{\mathbf{r}}V_r(\mathbf{x}_i)/H_0 - (1/2)\sigma^2_{pv}(\mathbf{x}_i)(\mathbf{J}\cdot\hat{\mathbf{r}})^2 H_0^2} \psi_{\mathbf{j},\mathbf{l}}(\mathbf{s})\Big|_{\mathbf{J}=0}.
\end{aligned}$$

For simplicity, we will use $\tilde{\epsilon}^S_{\mathbf{j},\mathbf{l}}$ for $\langle \tilde{\epsilon}^S_{\mathbf{j},\mathbf{l}} \rangle_v$ below without causing confusion.

If we consider only linear effect of the bulk velocity, equation (24) gives

$$\begin{aligned}
\tilde{\epsilon}^S_{\mathbf{j},\mathbf{l}} &= \sum_{i=1}^{N_g} w_i \int d\mathbf{s}\, \delta_D\left(\mathbf{s} - \mathbf{x}_i + i\nabla_J\right) \left[1 + i\frac{1}{H_0}\mathbf{J}\cdot\hat{\mathbf{r}}V_r(\mathbf{x}_i)\right] e^{-(1/2)\sigma^2_{pv}(\mathbf{x}_i)(\mathbf{J}\cdot\hat{\mathbf{r}})^2} \psi_{\mathbf{j},\mathbf{l}}(\mathbf{s})\Big|_{\mathbf{J}=0} \qquad (26)\\
&= \sum_{i=1}^{N_g} w_i \int d\mathbf{s} \psi_{\mathbf{j},\mathbf{l}}(\mathbf{s}) e^{-(1/2)\sigma^2_{pv}(\mathbf{s})(\hat{\mathbf{r}}\cdot\nabla)^2} \delta_D(\mathbf{s} - \mathbf{x}_i)\\
&- \frac{1}{H_0}\sum_{i=1}^{N_g} w_i \int d\mathbf{s}\, \hat{\mathbf{r}}\cdot[\nabla_s V_r(\mathbf{s} + i\nabla_J)\delta_D\left(\mathbf{s} - \mathbf{x}_i + i\nabla_J\right)] e^{-(1/2)\sigma^2_{pv}(\mathbf{x}_i)(\mathbf{J}\cdot\hat{\mathbf{r}})^2} \psi_{\mathbf{j},\mathbf{l}}(\mathbf{s})\Big|_{\mathbf{J}=0}
\end{aligned}$$

Neglecting the terms of the order of $V_r(\mathbf{x})\delta(\mathbf{x})$, and using the linear relation eq.(19), equation (26) gives

$$\begin{aligned}
\tilde{\epsilon}^S_{\mathbf{j},\mathbf{l}} &= \int d\mathbf{s} \psi_{\mathbf{j},\mathbf{l}}(\mathbf{s}) e^{(1/2)\sigma^2_{pv}(\mathbf{s})(\hat{\mathbf{r}}\cdot\nabla)^2} n^g(\mathbf{s}) \qquad (27)\\
&+ \beta \int d\mathbf{s} \psi_{\mathbf{j},\mathbf{l}}(\mathbf{s}) (\hat{\mathbf{r}}\cdot\nabla_s)^2 \nabla^{-2} e^{-(1/2)\sigma^2_{pv}(\mathbf{s})(\hat{\mathbf{r}}\cdot\nabla)^2} n^g(\mathbf{s})
\end{aligned}$$

Because all operators in the integrand of equation (27) are nearly diagonal in the DWT representation (Farge et al 1996), equation (27) can be rewritten as

$$\tilde{\epsilon}^S_{\mathbf{j},\mathbf{l}} = (1 + \beta S_{\mathbf{j}}) s^{pv}_{\mathbf{j}} \tilde{\epsilon}_{\mathbf{j},\mathbf{l}} \qquad (28)$$

where

$$S_{\mathbf{j}} = \int \psi_{\mathbf{j},\mathbf{l}}(\mathbf{x}) (\hat{\mathbf{r}}\cdot\nabla)^2 \nabla^{-2} \psi_{\mathbf{j},\mathbf{l}}(\mathbf{x}) d\mathbf{x}. \qquad (29)$$

and

$$s_{\mathbf{j}}^{pv} = \int \psi_{\mathbf{j},\mathbf{l}}(\mathbf{x}) e^{(1/2)\sigma_{pv}^2(\mathbf{x})(\hat{\mathbf{r}}\cdot\nabla)^2} \psi_{\mathbf{j},\mathbf{l}}(\mathbf{x}) d\mathbf{x} \tag{30}$$

The method of calculating $S_{\mathbf{j}}$ and $s_{\mathbf{j}}^{pv}$ is presented in Appendix A.

Substituting equation (28) into equation (22), we have the redshift distorted power spectrum as

$$P_{\mathbf{j}}^S = (1 + \beta S_{\mathbf{j}})^2 S_{\mathbf{j}}^{PV} P_{\mathbf{j}}. \tag{31}$$

where $S_{\mathbf{j}}^{PV} = [s_{\mathbf{j}}^{pv}]^2$. Above equation formulates the redshift distortion effect in DWT expression. This is the basic formula for our redshift distortion analysis. Usually, the factor $(1 + \beta S_{\mathbf{j}})^2$ is called linear redshift distortion, and $S_{\mathbf{j}}^{PV}$ called non-linear redshift distortion due to the pairwise velocity dispersion. However in our derivation, the two parts are not treated separately.

This derivation can be generalized to any velocity fields, which are not simply described by equations (18) and (20). For instance, if the pairwise velocities are correlated, i.e.

$$\langle [v_i(\mathbf{x}) - V_i(\mathbf{x})][v_i(\mathbf{x}') - V_i(\mathbf{x}')] \rangle_v = \sigma_{pv}^2(\mathbf{x} - \mathbf{x}'), \tag{32}$$

the pairwise velocity dispersion factor becomes

$$S_{\mathbf{j}}^{PV} = \int\int d\mathbf{x} d\mathbf{x}' \tag{33}$$
$$\psi_{\mathbf{j},\mathbf{l}}(\mathbf{x})\psi_{\mathbf{j},\mathbf{l}}(\mathbf{x}') e^{[(1/2)\sigma_{pv}^2(\mathbf{x})(\hat{\mathbf{r}}\cdot\nabla)^2 + \sigma_{pv}^2(\mathbf{x}-\mathbf{x}')(\hat{\mathbf{r}}\cdot\nabla)(\hat{\mathbf{r}}\cdot\nabla') + (1/2)\sigma_{pv}^2(\mathbf{x}')(\hat{\mathbf{r}}\cdot\nabla')^2]} \psi_{\mathbf{j},\mathbf{l}}(\mathbf{x})\psi_{\mathbf{j},\mathbf{l}}(\mathbf{x}'),$$

where ∇' is gradient operator on $\mathbf{x}'$.

3.3. Effect of selection functions

The theory of redshift distortion presented in last section did not consider the effects of selection functions, $\bar{n}^S(\mathbf{s})$ and $\bar{n}(\mathbf{s})$. Since selection function relies on the radial distance,

it could be also a source of the anisotropy of power spectrum with respect to redshift direction. It should be taken into account when analyze observed samples.

In the linear approximation of v_r, equation (21) gives

$$n^S(\mathbf{s}) = n^g(\mathbf{s}) - \sum_{i=1}^{N_g} \frac{1}{H_0} v_r(\mathbf{x_i}) \hat{\mathbf{r}} \cdot \nabla \delta_D(\mathbf{s} - \mathbf{x}_i) = n^g(\mathbf{s}) - \frac{1}{H_0} \hat{\mathbf{r}} \cdot \nabla [n^g(\mathbf{s}) V_r(\mathbf{s})]. \tag{34}$$

In the second steps, v_r is replaced by V_r, as only the bulk velocity is considered. Using equations (1) and (21), equation (34) yields

$$\delta^S(\mathbf{s}) \simeq -1 + \frac{\bar{n}(\mathbf{s})}{\bar{n}^S(\mathbf{s})} + \frac{\bar{n}(\mathbf{s})}{\bar{n}^S(\mathbf{s})} \left\{ \delta(\mathbf{s}) - \frac{1}{H_0 \bar{n}(\mathbf{s})} \hat{\mathbf{r}} \cdot \nabla [\bar{n}(\mathbf{s}) V_r(\mathbf{s})] \right\}, \tag{35}$$

where the second order term $\delta(\mathbf{s}) V_r(\mathbf{s})$ is ignored.

The term -1 on the r.h.s. of equation (35) does not contribute to power spectrum, because of $\int \psi_{\mathbf{j},\mathbf{l}}(x) dx = 0$. In the linear approximation, $\bar{n}(\mathbf{s})/\bar{n}^S(\mathbf{s}) \simeq 1 + O(v_r)$ and therefore, the factor $\bar{n}^g(\mathbf{s})/\bar{n}^S(\mathbf{s})$ in the third term of the r.h.s. of equation (34) can be approximated as 1.

The second term in the r.h.s. of equation (35) contains a linear term of V_r, i.e. the same order as the third term. However, with the selection function equation (13), we have

$$\int \bar{n}^g(\mathbf{x}) \psi_{\mathbf{j},\mathbf{l}}(\mathbf{x}) d\mathbf{x} = \int \bar{n}^{(\mathbf{j}')}(\mathbf{x}) \psi_{\mathbf{j},\mathbf{l}}(\mathbf{x}) d\mathbf{x} = 0 \;\; \text{if one of } j_i \; (i = 1, 2, 3) \text{ satisfies } \; j_i \geq j'_i. \tag{36}$$

For plane parallel approximation, $\mathbf{j}' = (0, 0, j'_3)$, the above equation is always hold if we study fluctuation powers on scales $j_1 > 0$ or $j_2 > 0$. Actually, in this case, $\bar{n}^g(\mathbf{x})$ or $\bar{n}^{(\mathbf{j}')}(\mathbf{x})$ depend only on x_3, and thus their projections onto bases $\psi_{j,l}(x_1)$ or $\psi_{j,l}(x_2)$ $(j > 0)$ are always null. Similarly the selection function in redshift space is also only dependent on x_3. Accordingly, in the plane parallel approximation, we have

$$\int \frac{\bar{n}(\mathbf{s})}{\bar{n}^S(\mathbf{s})} \psi_{\mathbf{j},\mathbf{l}} d\mathbf{s} = 0 \;\; \text{if} j_1 \text{ or } j_2 > 0. \tag{37}$$

which implies that the second term in the r.h.s. of equation (34) also has not contribution to the projection on bases $\psi_{\mathbf{j},\mathbf{l}}(x_1)$ or $\psi_{\mathbf{j},\mathbf{l}}(x_2)$.

In fact, the condition of plane parallel approximation is not necessary. For radial redshift, the selection function is still a 1-D function. Its projection onto the bases $\psi_{\mathbf{j},\mathbf{l}}$ on the celestial spherical surface is still zero. Thus, the linear redshift distortion mapping is given by

$$\delta^S(\mathbf{s}) \simeq \delta(\mathbf{s}) - \frac{1}{H_0 \bar{n}(\mathbf{s})} \hat{r} \cdot \nabla[\bar{n}(\mathbf{s}) v_r(\mathbf{s})]. \tag{38}$$

Hereafter we will use $\mathbf{x}$ for the variable $\mathbf{s}$. It will not cause confusion as the superscript S stands for redshift space.

In the plane parallel approximation, equation (38) becomes

$$\delta^S(\mathbf{x}) = \delta(\mathbf{x}) - \frac{1}{H_0}\frac{\partial v_3}{\partial x_3} - \frac{1}{H_0}\frac{d \ln \bar{n}(x_3)}{dx_3} v_3(\mathbf{x}), \tag{39}$$

Using equation (19), v_3 can be represented by $\delta(\mathbf{x})$, we have then

$$\delta^S(\mathbf{x}) = \left[1 + \beta \frac{\partial^2}{\partial x_3^2}\nabla^{-2} + \beta \frac{d \ln \bar{n}(x_3)}{dx_3}\frac{\partial}{\partial x_3}\nabla^{-2}\right]\delta(\mathbf{x}). \tag{40}$$

The differential operator of the second term in the bracket of equation (40) is nearly diagonal in the DWT representation (Farge et al 1996.) Thus, we have

$$\tilde{\epsilon}^S{}_{\mathbf{j},\mathbf{l}} \simeq (1 + \beta S_{\mathbf{j}})\tilde{\epsilon}_{\mathbf{j},\mathbf{l}} + \beta \left.\frac{d \ln \bar{n}(x_3)}{dx_3}\right|_{\mathbf{j},\mathbf{l}} \sum_{l_3 - l'_3} Q_{\mathbf{j},l_3-l'_3}\tilde{\epsilon}_{\mathbf{j},l_1,l_2,l'_3} \tag{41}$$

where $d \ln \bar{n}^S(x_3)/dx_3|_{\mathbf{j},\mathbf{l}}$ means the value of $d \ln \bar{n}^S(x_3)/dx_3$ in the mode $\mathbf{j},\mathbf{l}$. The coefficient $Q_{\mathbf{j},l_3-l'_3}$ are defined by

$$Q_{\mathbf{j},l_3-l'_3} = \int \psi_{\mathbf{j},l_1,l_2,l_3}(\mathbf{x})\frac{\partial}{\partial x_3}\nabla^{-2}\psi_{\mathbf{j},l_1,l_2,l'_3}(\mathbf{x})d\mathbf{x}. \tag{42}$$

The calculations of $Q_{\mathbf{j},l_3-l'_3}$ are given in Appendix A.

Since $Q_{\mathbf{j},0} = 0$ (Appendix A), the first and second terms on the r.h.s. of equation (40) are not correlated, we have

$$\langle|\tilde{\epsilon}^S{}_{\mathbf{j},\mathbf{l}}|^2\rangle = [1 + \beta S_{\mathbf{j}}]^2\langle|\tilde{\epsilon}_{\mathbf{j},\mathbf{l}}|^2\rangle + \left[\beta \left.\frac{d \ln \bar{n}(x_3)}{dx_3}\right|_{\mathbf{j},\mathbf{l}}\right]^2 \sum_{l_3-l'_3} Q^2_{\mathbf{j},l_3-l'_3}\langle|\tilde{\epsilon}_{\mathbf{j},l_1,l_2,l'_3}|^2\rangle \tag{43}$$

For uniform fields, $\langle|\tilde{\epsilon}^S{}_{\mathbf{j},\mathbf{l}}|^2\rangle$ and $\langle|\tilde{\epsilon}_{\mathbf{j},\mathbf{l}}|^2\rangle$ are **l**-independent. Hence, equation (43) gives the relation between the DWT power spectra in redshift $P^S_{\mathbf{j}}$ and real spaces $P_{\mathbf{j}}$ as

$$P^S_{\mathbf{j}} = \left\{ [1+\beta S_{\mathbf{j}}]^2 + \left[\beta \frac{d\ln\bar{n}(x_3)}{dx_3}\bigg|_{\mathbf{j},\mathbf{l}} \right]^2 \sum_{l_3-l'_3} Q^2_{\mathbf{j},l_3-l'_3} \right\} P_{\mathbf{j}}. \tag{44}$$

which quantifies both redshift distortion and selection effect on the DWT power spectrum.

Using inequality equation (A15), we can show that if

$$\frac{d\ln\bar{n}(x_3)}{dx_3} < 2\pi n_p \frac{2^{j_3}}{L_3}, \tag{45}$$

we have

$$\left[\beta \frac{d\ln\bar{n}(x_3)}{dx_3}\bigg|_{\mathbf{j},\mathbf{l}} \right]^2 \sum_{l_3-l'_3} Q^2_{\mathbf{j},l_3-l'_3} < \beta^2 S^2_{\mathbf{j}}. \tag{46}$$

which states that the selection function term in equation (44) is even less than the second order terms $\beta^2 S^2_{\mathbf{j}}$ if the selection function varies with x_3 slowly. In this case, the selection function does not significantly disturb the linear redshift distortion described by equation (31) when we perform a DWT power spectrum analysis using equations (10) and (15).

The Poisson noise term in equation (10) is not affected by the redshift distortion, i.e. it is the same as the Poisson noise term in equation (22). Because both Poisson noise terms of equations (10) and (22) linearly depend on $n(\mathbf{x})$ or $n^S(\mathbf{x})$, for an ensemble average, we have $\langle n(\mathbf{x})\rangle = \langle n^S(\mathbf{x})\rangle$.

4. Simulation samples

To demonstrate the redshift distortion in the DWT representation, we use the N-body simulation samples like that in Paper II. The model parameters used are listed in table. 1. We use modified AP^{3}M code (Couchman, 1991) to evolve 128^3 cold dark matter particles in a periodic cube of side length L. The linear power spectrum is using the fitting formula given in Bardeen et al. (1986).

In our simulation, we use the so-called "glass" configuration to generate the unperturbed uniform distribution of particles, and the Zel'dovich approximation to set up the initial perturbation. The triangular-shaped cloud (TSC) method is used for the mass assignment on the grid and the calculation of the force on a given particle from interpolation of the grid values. We take 600 total integration steps from $z_i = 15$ for the SCDM model, and $z_i = 25$ for ΛCDM and τCDM down to $z = 0$. The force softening parameter η in the comoving system decreases with time as $\eta \propto 1/a(t)$. Its initial value is taken to be 15%, and the minimum value to be 5% of the grid size, respectively.

5. β-estimators and reconstruction

5.1. A test of the linear approximation

We try to estimate the redshift distortion parameter β using equation (30). Obviously, the precision of the β determination is dependent on the linear relation of equation (18), which is valid only on the scales where the bulk velocity can be described by linear or quasi-linear density perturbations. It has been already realized that the non-linearity of the relation between $\delta(\mathbf{x})$ and $\mathbf{V}(\mathbf{x})$ will be significant on small scales (e.g. Kudlicki et al.

Table 1

Model	L/h^{-1}Mpc	Ω_0	Λ	Γ	σ_8	β	realizations
SCDM	256	1.0	0.0	0.5	0.55	1.0	10
τCDM	256	1.0	0.0	0.25	0.55	1.0	10
ΛCDM1	256	0.3	0.7	0.21	0.85	0.49	10
ΛCDM2	480	0.3	0.7	0.21	0.95	0.49	6

2000). Therefore, it is necessary to have an estimation of uncertainties due to the non-linear $\delta(\mathbf{x}) - \mathbf{V}(\mathbf{x})$ relation.

The non-linear effect can be estimated by a "blueshift" (change the sign of velocity from $\mathbf{v}(\mathbf{x})$ to $-\mathbf{v}(\mathbf{x})$) distorted power spectrum. From the derivation of equation (31) in last section, it is easy to show that, the blueshifted power spectrum is

$$P^B_{\mathbf{j}} = (1 - \beta S_{\mathbf{j}})^2 S^{PV}_{\mathbf{j}} P_{\mathbf{j}}. \tag{47}$$

Which has the same non-linear redshift distortion effect $S^{PV}_{\mathbf{j}}$ as the redshift power spectrum. The difference between the redshift [equation (31)] and blueshift [equation (47)] distorted power spectra is a sign of the linear term β. Combining equations (31) and (47), one can determine β as

$$\beta = \frac{1}{S_{\mathbf{j}}} \frac{(\sqrt{P^S_{\mathbf{j}}} - \sqrt{P^B_{\mathbf{j}}})}{(\sqrt{P^S_{\mathbf{j}}} + \sqrt{P^B_{\mathbf{j}}})}. \tag{48}$$

We test equation (48) by simulation samples in the ΛCDM model. First, we calculate the diagonal power spectra of particles, P^S_{jjj} and P^B_{jjj}, in the plane parallel approximation. We then find β by equation (48). The result is presented in Fig. 2. The density parameter used for the simulation is $\Omega = 0.3$, or $\beta = 0.49$. Fig. 2 shows that the values of β given by equation (48) is generally overestimated. But the overestimations are no more than 10% on scales $k < 0.5$ h Mpc^{-1}, and about 20% for $k > 1$ h Mpc^{-1}. It should be pointed out that the goodness of the resulted β on small scales $k > 1$ h Mpc^{-1} doesn't mean that the linear relation eq.(19) can be used to describe the redshift distortion on these scales. The non-linear effect on these scales can not be ignored, and the redshift distortion is dominated by the term $S^{PV}_{\mathbf{j}}$. The goodness for $k > 1$ h Mpc^{-1} shown in Fig. 2 is due to that the non-linear effect is significantly repressed by the test eq.(48) based on an assumed blueshifts.

5.2. Symmetry of the DWT quantities

At the first glance, it seems impossible to estimate β using the observed redshift distorted power spectrum $P^S_{\mathbf{j}}$ only, as all the quantities such as β, $P_{\mathbf{j}}$, and $S^{PV}_{\mathbf{j}}$ (or σ_{pv}) included on the r.h.s. of equation (30) are unknown. Usually, equation (30) is used to fit the observed power spectrum with model-predicted $P_{\mathbf{j}}$, and then determine the parameter β from the most-likely-fitting.

But we try to search for β-estimators which depend on model as less as possible. To achieve this, we take the advantage of the wavelet analysis: the DWT modes of $\psi_{j_1,j_2,j_3}(\mathbf{x})$ are not rotational invariant, but cyclic permutational invariant. As a consequence, all the DWT quantities in the redshift distortion equation (30), $P_{\mathbf{j}}$, $P^S_{\mathbf{j}}$, $S_{\mathbf{j}}$, and $S^{PV}_{\mathbf{j}}$, are dependent on the three indexes (j_1, j_2, j_3), rather than the length scale of mode $\mathbf{j}$ only. The quantities $P_{\mathbf{j}}$, $P^S_{\mathbf{j}}$, $S_{\mathbf{j}}$ and $S^{PV}_{\mathbf{j}}$ satisfy the following symmetry.

1. If cosmic density and velocity fields are statistically isotropic, the DWT power spectrum in real space is invariant with respect to the cyclic permutations of index $\mathbf{j} = (j_1, j_2, j_3)$, i.e.

$$P_{j_1,j_2,j_3} = P_{j_3,j_1,j_2} = P_{j_2,j_3,j_1} \tag{49}$$

2. In the plane-parallel approximation, e.g., coordinate x_3 is in the redshift direction, we have

$$P^S_{j_1,j_2,j_3} = P^S_{j_2,j_1,j_3} \tag{50}$$

$$S_{j_1,j_2,j_3} = S_{j_2,j_1,j_3} \tag{51}$$

$$S^{PV}_{j_1,j_2,j_3} = S^{PV}_{j_2,j_1,j_3} \tag{52}$$

3. If σ_{pv} is constant, i.e. scale-independent, following equation (A10), we have

$$S^{PV}_{j_1,j_2,j_3} = S^{PV}_{j_3}, \tag{53}$$

i.e. $S_{\mathbf{j}}^{PV}$ is independent of j_1 and j_2. More generally, equation (53) also hold even when the radial correlation of pairwise peculiar velocity is considered [equation (33)].

Equations (49) - (53) provide the base of designing the β-estimators with the DWT power spectrum.

5.3. β-estimator with scale-independent σ_{pv}

Assuming that the pairwise velocity dispersion is scale-independent, equations (31) and (49) give

$$\frac{P^S_{jj_2j_3}}{P^S_{jj_3j_2}} \simeq \frac{(1+\beta S_{jj_2j_3})^2}{(1+\beta S_{jj_2j_3})^2}\left[\frac{S^{PV}_{jj_2j_3}}{S^{PV}_{jj_3j_2}}\right]^2. \tag{54}$$

For a given pair (j_2, j_3), $S^{PV}_{jj_2j_3}/S^{PV}_{jj_3j_2}$ is a constant, and thus the r.h.s. of equation (54) depends only on two parameters β and $S^{PV}_{jj_2j_3}/S^{PV}_{jj_3j_2}$. Accordingly, these parameters can be found by the best fitting of the r.h.s. of equation (54) with observed ratios $P^S_{jj_2j_3}/P^S_{jj_3j_2}$, $j = 2, 3...$

A numerical example of this fitting is demonstrated in Fig. 3, in which we take $(j_2, j_3) = (2, 3)$, and $j = 2...7$. We calculate $P^S_{jj_2j_3}/P^S_{jj_3j_2}$ for the ΛCDM simulation samples, and the best fitting yields the values of $\beta = 0.53 \pm 0.25$ and $S^{PV}_{j23}/S^{PV}_{j32} = 0.80 \pm 0.04$. The precision of the estimator eq.(53) probably is not better than 20%. This shows that the assumption of a constant σ_{pv} is not too bad, but its effect on the β-determination cannot be neglected.

5.4. β-Estimator with scale-dependent σ_{pv}

If σ_{pv} is scale-dependent, equation (54) is no longer correct in general. In this case $S^{PV}_{j_1,j_2,j_3}$ depends on the three index (j_1, j_2, j_3), rather than j_3 only. So the relation eq.(30)

is obviously not enough to extract β from measuring redshift distorted power spectrum $P^S_{\mathbf{j}}$ only. To search for an appropriate algorithm for β estimation, we shall first consider the property of $S^{PV}_{\mathbf{j}}$.

At first, the pairwise velocity dispersion factor $S^{PV}_{\mathbf{j}}$ is determined by an isotropic function $\sigma_{pv}(\mathbf{x})$, which is scale-dependent. Let us consider the modes of $L/2^{j_\perp} < L/2^{j_3}$, where $j_\perp$ is defined by $2^{2j_\perp} \equiv 2^{2j_1} + 2^{2j_2}$. In this case, the scales of these modes are dominant by j_3, and therefore, $\sigma_{pv}(\mathbf{x})$ is also dominant by j_3. That is, for a given j_3, $S^{PV}_{\mathbf{j}}$ will keep constant if $j_\perp > j_3$.

To test this expectation, we calculate $S^{PV}_{\mathbf{j}}$ in the ΛCDM model. The result is shown in Fig. 4. One can see from Fig. 4 that $S^{PV}_{\mathbf{j}}$ is generally dependent on indexes $j_\perp$ as well as j_3. However, for a given j_3, $S^{PV}_{\mathbf{j}}$ almost keeps constant in the range of $j_\perp > j_3$. Since $j = 2, 3$ is the two largest scales of the samples, $S^{PV}_{j_1 j_2 2}$ and $S^{PV}_{j_1 j_2 3}$ keep constant very well for all j_1, j_2.

Using this result, we can design a β-estimator as follows

$$\frac{P^S_{j23} P^S_{j'32}}{P^S_{j'23} P^S_{j32}} = \frac{(1+\beta S_{j23})^2 (1+\beta S_{j'32})^2}{(1+\beta S_{j'23})^2 (1+\beta S_{j32})^2}, \tag{55}$$

or

$$\beta \simeq \left[\left(\frac{P^S_{j23} P^S_{j'32}}{P^S_{j'23} P^S_{j32}} \right)^{1/2} - 1 \right] \frac{1}{(S_{j23} - S_{j32} + S_{j'32} - S_{j'23})} \tag{56}$$

Obviously, the first factor on the r.h.s. of equation (56) is to measure the difference between spectra with the same scales, but different shapes of the modes. The estimator eq.(56) is model-free, as equation (56) is based only on property that two DWT modes of $(j_\perp, j_3)$ and $(j'_\perp, j_3)$ have the same scale, but different shapes if $j_\perp > j_3$ and $j'_\perp > j_3$.

To apply the estimator (56), we take $j = 2$ and $j' = 7$, because modes with $j = 2$ and $j' = 7$ have largest difference in the shape, but very small difference in the scale. This estimator yields the values of $\beta = 0.47 \pm 0.18$ for ΛCDM sample with simulation box $L =$ 480 h^{-1} Mpc; 0.93 ± 0.22 for SCDM sample with $L = 256$ h^{-1} Mpc; and 1.00 ± 0.34 for

τCDM sample with $L = 256$ h^{-1} Mpc. Considering the uncertainty of non-linearity is about 20% (§5.1), the estimator eq. (56) works very well.

5.5. Estimation of σ_{pv}

After the β estimation, we can also estimate σ_{pv} on scale j_3 using off-diagonal power spectrum in redshift space. From §5.4, we know that $S^{PV}_{\mathbf{j}}$ is almost constant in the range of $j_\perp > j_3$. So we have $S^{PV}_{77j} = S^{PV}_{jjj}$ and $S^{PV}_{j77} = S^{PV}_{777}$.

We can calculate the ratio of pairwise velocity dispersion factor $S^{PV}_{jjj}/S^{PV}_{777}$ by

$$\frac{P^S_{77j}(1+\beta S_{j77})^2}{P^S_{j77}(1+\beta S_{77j})^2} = \frac{S^{PV}_{77j}}{S^{PV}_{j77}} = \frac{S^{PV}_{jjj}}{S^{PV}_{777}}. \tag{57}$$

On the largest scale $j = 2$, the nonlinear redshift distortion due to the pairwise velocity dispersion is negligible, we have $S^{PV}_{222} \simeq 1$. Thus, we have all the diagonal members of the pairwise velocity dispersion factor S^{PV}_{jjj}. The parameter σ_{pv} on the scale j can then be found by $S^{PV}_{jjj} = [s^{pv}_{jjj}]^2$ with equation (A10), i.e.

$$s^{pv}_{j_1,j_2,j_3} = \frac{1}{2^{j_3}} \sum_{n_3=\infty}^{\infty} |\hat{\psi}(n_3/2^{j_3})|^2 \exp[-(1/2)\sigma^2_{pv}(2\pi n_3/L_3)^2]. \tag{58}$$

For the ΛCDM simulation sample, S^{PV}_{jjj} is shown in Fig.5. The σ_{pv} on scales $j = 3...7$ is shown in Fig. 6. Although the values of σ_{pv} shown in Fig. 6 are correct in average, but it does not match with the direct measurement of σ_{pv} given in Paper III. Especially, on small scales $j = 6$ and 7, the values of σ_{pv} are significantly lower than the direct measurement. This is not unexpected. The factor $s^{pv}_{\mathbf{j}}$ equation (58) is obtained under the assumption of gaussian velocity field (§3.1). However, we have shown in Paper III that the velocity field is actually intermittent on small scales. The PDF of $\tilde{\epsilon}^v_{\mathbf{j},\mathbf{l}}$ is not gaussian, but lognormal.

Nevertheless, the factor $S^{PV}_{\mathbf{j}}$ is still good for the redshift-real mapping and β-estimation, because in these calculations, we used only the symmetric properties and scale-dependence

of $S_{\mathbf{j}}^{PV}$, but not the details of σ_{pv}. This point can also be seen from reconstruction of power spectrum in real space from that in redshift space. Using the β estimated by equation (56), and S_{jjj}^{PV} by equation (57), one can reconstruct the diagonal DWT power spectrum in real space P_{jjj} from P_{jjj}^S through equation (31). Fig.(7) compares the recovery of P_{jjj} with the original diagonal DWT power spectrum in the ΛCDM model. The result shows that the algorithm of reconstruction is reliable.

6. Conclusion

We established the mapping between the DWT power spectra in real and redshift spaces. From equations (31) and (44), the mapping in the plane parallel approximation is

$$P_{\mathbf{j}}^S = \left\{ [1+\beta S_{\mathbf{j}}]^2 + \left[\beta \frac{d\ln \bar{n}(x_3)}{dx_3}\bigg|_{\mathbf{j},\mathbf{l}} \right]^2 \sum_{l_3-l_3'} Q_{\mathbf{j},l_3-l_3'}^2 \right\} S_{\mathbf{j}}^{PV} P_{\mathbf{j}}. \tag{59}$$

which includes the effects of (1) bulk velocity (the term of $S_{\mathbf{j}}$), and (2) selection function (the term of $\bar{n}(x_3)$) as well as (3) pairwise peculiar velocity (the term of $S_{\mathbf{j}}^{PV}$).

In the Fourier representation, the redshift distortion mapping is axially symmetric with respect to the redshift direction. This is because the Fourier mode is rotational invariant, and the redshift distortion produces an anisotropy in the spatial distribution of galaxies between the line of sight and directions other than it. An isotropic statistics plus an axially symmetric violation will result in an axial symmetry. On the other hand, all redshift distortion factors in equation (59) are no longer axial symmetric, which is due to the modes **j** being not invariant under rotational transformation, but for cyclical permutation. Therefore, the symmetry of the DWT redshift distortion results from a cyclical permutation plus an axially symmetric violation.

By virtue of this feature, we develop β estimators, which are mainly based on the shape-dependence of the redshift distorted DWT power spectrum, but not the scale-dependence.

The estimators eqs.(54) and (56) look similar to the quadrupole-to-monopole ratio method based on the Fourier power spectrum in redshift space, which gives a model-free estimation of β (e.g. Cole et al, 1994, Fisher et al, 1994, Hatton & Cole, 1998, Szalay et al, 1998). However, the estimators eqs.(54) and (56) is different from the quadrupole-to-monopole ratio method. The latter considered only the linear redshift distortion effect, but not the non-linear redshift distortion effect. If considering the non-linear redshift distortion effect, the quadrupole-to-monopole ratio method needs a fitting of observed redshift distorted power spectrum with model-predicted power spectrum. On the other hand, the estimators eqs.(54) and (56) considered both linear ($\beta S_{\mathbf{j}}$) and non-linear ($S_{\mathbf{j}}^{PV}$) redshift distortion effects. These β-estimators are model-free even when the non-linear redshift distortion effect is not negligible. We test the β-estimators using N-body simulation samples. The result shows that regardless the pairwise velocity dispersion is scale-dependent or not, the β-estimators can yield the correct number of β with about 20% uncertainty. We also develop an algorithm for reconstruction of the power spectrum in real space from the redshift distorted power spectrum. The numerical tests also show that the real power spectrum can be reasonably recovered from the redshift distorted power spectrum.

LLF and YQC acknowledges support from the National Science Foundation of China (NSFC) and National Key Basic Research Science Foundation.

A. Calculations of $S_{\mathbf{j}}$, $s_{\mathbf{j}}^{pv}$, and $Q_{\mathbf{j},\mathbf{l}-\mathbf{l}'}$

A.1. $S_{\mathbf{j}}$

Let us consider plane-parallel approximation, i.e. coordinate x_3 is in the redshift (z)-direction. The linear redshift distortion $S_{\mathbf{j}}$ equation (28) gives

$$S_{\mathbf{j}} = \int \psi_{\mathbf{j},\mathbf{l}}(\mathbf{x}) \frac{\partial^2}{\partial x_3^2} \nabla^{-2} \psi_{\mathbf{j},\mathbf{l}}(\mathbf{x}) d\mathbf{x}. \tag{A1}$$

Because 1-D wavelet $\psi_{j,l}(x)$ is given by dilating and translating the basic wavelet $\psi(\eta)$ as

$$\psi_{j,l}(x) = \left(\frac{2^j}{L}\right)^{1/2} \psi(\frac{2^j x}{L} - l), \tag{A2}$$

The Fourier transform of $\psi_{j,l}$ is

$$\psi_{j,l} = \frac{1}{L} \sum_{n=-\infty}^{\infty} \hat{\psi}_{j,l}(n) e^{-i2\pi nx/L} \tag{A3}$$

and

$$\hat{\psi}_{j,l}(n) = \left(\frac{L}{2^j}\right)^{1/2} \hat{\psi}(n/2^j) e^{-i2\pi nl/2^j}, \tag{A4}$$

where $\hat{\psi}(n)$ is the Fourier transform of the basic wavelet

$$\hat{\psi}(n) = \int_{-\infty}^{\infty} \psi(\eta) e^{-i2\pi n\eta} d\eta. \tag{A5}$$

The function $|\hat{\psi}(n)|^2$ is shown in Fig. 1 of Yang et al. (2001).

Thus, equation (A1) becomes

$$\begin{aligned} S_{j_1,j_2,j_3} &= \frac{1}{2^{j_1+j_2+j_3}} \\ &\sum_{n_1,n_2,n_3=\infty}^{\infty} \frac{(n_3/L_3)^2}{(n_1/L_1)^2 + (n_2/L_2)^2 + (n_3/L_3)^2} |\hat{\psi}(n_1/2^{j_1}) \hat{\psi}(n_2/2^{j_2}) \hat{\psi}(n_3/2^{j_3})|^2. \end{aligned} \tag{A6}$$

Since $\hat{\psi}(n)$ is non-zero only around two peaks at $n = \pm n_p$, the summation of equation (A6) actually only over few number of n_i around $\pm n_p 2^{j_i}$.

If $L_1 = L_2 = L_3 = L$, equation (A6) becomes

$$S_{j_1,j_2,j_3} = \frac{1}{2^{j_1+j_2+j_3}} \sum_{n_1,n_2,n_3=\infty}^{\infty} \frac{n_3^2}{n_1^2 + n_2^2 + n_3^2} |\hat{\psi}(n_1/2^{j_1}) \hat{\psi}(n_2/2^{j_2}) \hat{\psi}(n_3/2^{j_3})|^2. \tag{A7}$$

For diagonal modes, i.e. $j_1 = j_2 = j_3 = j$ we have

$$S_{j,j,j} = \frac{1}{3} \tag{A8}$$

A.2. $s^{pv}_{\mathbf{j}}$

If $\sigma_v(\mathbf{x})$ is independent of $\mathbf{x}$, $s^{pv}_{\mathbf{j}}$ [equation (28)] can be calculated by

$$s^{pv}_{j_1,j_2,j_3} = \frac{1}{2^{j_1+j_2+j_3}} \sum_{n_1,n_2,n_3=\infty}^{\infty} |\hat{\psi}(n_1/2^{j_1})\hat{\psi}(n_2/2^{j_2})\hat{\psi}(n_3/2^{j_3})|^2 \exp[-(1/2)\sigma^2_{pv}(\hat{r}\cdot\mathbf{n})^2], \tag{A9}$$

where vector $\mathbf{n} = 2\pi(n_1/L_1, n_2/L_2, n_3/L_3)$. In plane-parallel approximation, we have

$$s^{pv}_{j_1,j_2,j_3} = \frac{1}{2^{j_3}} \sum_{n_3=\infty}^{\infty} |\hat{\psi}(n_3/2^{j_3})|^2 \exp[-(1/2)\sigma^2_{pv}(2\pi n_3/L_3)^2]. \tag{A10}$$

The summation of equations. (A9) and (A10) also runs only over few number of n_i around $\pm n_p 2^{j_i}$.

A.3. $Q_{\mathbf{j},\mathbf{l}-\mathbf{l}'}$

Similarly, for $Q_{\mathbf{j},\mathbf{l}-\mathbf{l}'}$ given by [equation (41)]

$$Q_{\mathbf{j},l_3-l'_3} = \int \psi_{\mathbf{j},l_1,l_2,l_3}(\mathbf{x}) \frac{\partial}{\partial x_3} \nabla^{-2} \psi_{\mathbf{j},l_1,l_2,l'_3}(\mathbf{x}) d\mathbf{x}, \tag{A11}$$

we have

$$Q_{\mathbf{j},l_3-l'_3} = \frac{1}{2^{j_1+j_2+j_3}} \tag{A12}$$
$$\sum_{n_1,n_2,n_3=\infty}^{\infty} \frac{(n_3/L_3)\sin[2\pi n_3(l_3-l'_3)/2^{j_3}]}{2\pi[(n_1/L_1)^2+(n_2/L_2)^2+(n_3/L_3)^2]} |\hat{\psi}(n_1/2^{j_1})\hat{\psi}(n_2/2^{j_2})\hat{\psi}(n_3/2^{j_3})|^2.$$

Equation.(A12) gives

$$Q_{\mathbf{j},l_3-l'_3} = 0, \quad \text{if} \quad l_3 - l'_3 = 0. \tag{A13}$$

From equation (A12), we have

$$
\begin{aligned}
Q_{\mathbf{j},\mathbf{l}-\mathbf{l}'} &= \frac{1}{2^{j_1+j_2+j_3}} \qquad \text{(A14)}\\
&\sum_{n_1,n_2,n_3=\infty}^{\infty} \frac{L_3}{n_3} \frac{(n_3/L_3)^2 \sin[2\pi n_3(l_3-l_3')/2^{j_3}]}{2\pi[(n_1/L_1)^2+(n_2/L_2)^2+(n_3/L_3)^2]} |\hat{\psi}(n_1/2^{j_1})\hat{\psi}(n_2/2^{j_2})\hat{\psi}(n_3/2^{j_3})|^2.\\
&\simeq \frac{L_3}{2\pi n_p 2^{j_3}} \frac{1}{2^{j_1+j_2+j_3}}\\
&\sum_{n_1,n_2,n_3=\infty}^{\infty} \frac{(n_3/L_3)^2 \sin[2\pi n_3(l_3-l_3')/2^{j_3}]}{[(n_1/L_1)^2+(n_2/L_2)^2+(n_3/L_3)^2]} |\hat{\psi}(n_1/2^{j_1})\hat{\psi}(n_2/2^{j_2})\hat{\psi}(n_3/2^{j_3})|^2,
\end{aligned}
$$

for the last step, we consider that $\hat{\psi}(n_3/2^{j_3})$ requires $n_3 \simeq 2^{j_3} n_p$, and $n_p \simeq 1$ being the peak of $\hat{\psi}(n)$. Since $\sum_{l=0}^{2^j-1} \sin(2\pi nl/2^j) < 1$, equations.(A7) and (A14) yield

$$
\sum_{l_3-l_3'} Q^2_{\mathbf{j},l_3-l_3'} < \left(\frac{L_3}{2\pi n_p 2^{j_3}}\right)^2 S^2_{\mathbf{j}}. \qquad \text{(A15)}
$$

REFERENCES

Bardeen, J.M., Bond, J.R., Kaiser, N. & Szalay, A.S., 1986, ApJ, 304, 15

Cole, S., Fisher, K.B. & Weinberg, D.H., 1994, MNRAS, 267, 785

Couchman, H.M.P., 1991, ApJ, 368, 23

Daubechies I. 1992, Ten Lectures on Wavelets, (Philadelphia, SIAM)

Fang, L.Z. & Thews, R. 1998, Wavelet in Physics, (World Scientific, Singapore)

Fang, L.Z. & Feng, L.L. 2000, ApJ, 539, 5 (paper I).

Fisher, K.B., Scharf, C.A. & Lahav, O., 1994, MNRAS, 266, 219

Hamilton, A.J.S., 1998, The Evolving Universe, (Kluwer Academic Publisher, Germany)

Hatton, S.J. & Cole, S., 1998 MNRAS, 296, 10

Jamkhedkar, P., Bi, H.G. & Fang, L.Z. 2001, ApJ, in press, astr-ph/0107185

Kaiser, N. 1987, MNRAS, 227, 1

Kudlicki, A., Chodorowski, M.J., Plewa, T. & Rózyczka, M. 2000, MNRAS, 316, 464

Peacock, J.A. & Dodds, S.J., 1994, MNRAS, 167, 1020

Szalay, A.S., Matsubara, T. & Landy, S.D., 1998, ApJ, 498, L1

Yang, X.H., Feng, L.L., Chu, Y.Q. & Fang, L.Z. 2001a, ApJ, 553, 1 (paper II).

Yang, X.H., Feng, L.L., Chu, Y.Q. & Fang, L.Z. 2001b, ApJ, in press (paper III).

This manuscript was prepared with the AAS LaTeX macros v4.0.

Fig. 1.— The diagonal DWT power spectrum (square) measured in simulation samples for models SCDM (upper panel), τCDM (central panel) and ΛCDM1 (lower panel). The error bars are 1-σ variance from 10 realizations for each model. The solid lines are the original power spectrum

Fig. 2.— The values of β estimated by the redshift and blueshift power spectra in the ΛCDM2 simulation samples. The error bars are 1-σ variance from 6 realizations.

Fig. 3.— $P^S_{jj_2j_3}/P^S_{jj_3j_2}$ vs. j of ΛCDM2 simulation samples. The error bars are 1-σ variance from 6 realizations. The solid line is given by a best fitting with eq.(52)

Fig. 4.— $S^{PV}_{\mathbf{j}}$ vs. $j_\perp$ of ΛCDM2 simulation samples. The error bars are 1-σ variance from 6 realizations.

Fig. 5.— $S^{PV}_{jjj}/S^{PV}_{222}$ of ΛCDM2 simulation samples. The error bars are 1-σ variance from 6 realizations.

Fig. 6.— PVD estimated from the ΛCDM2 simulation samples. The error bars are 1-σ variance from 6 realizations for each model.

Fig. 7.— Reconstructed DWT power spectrum for the ΛCDM2 simulation samples. The error bars are 1-σ variance from 6 realizations.

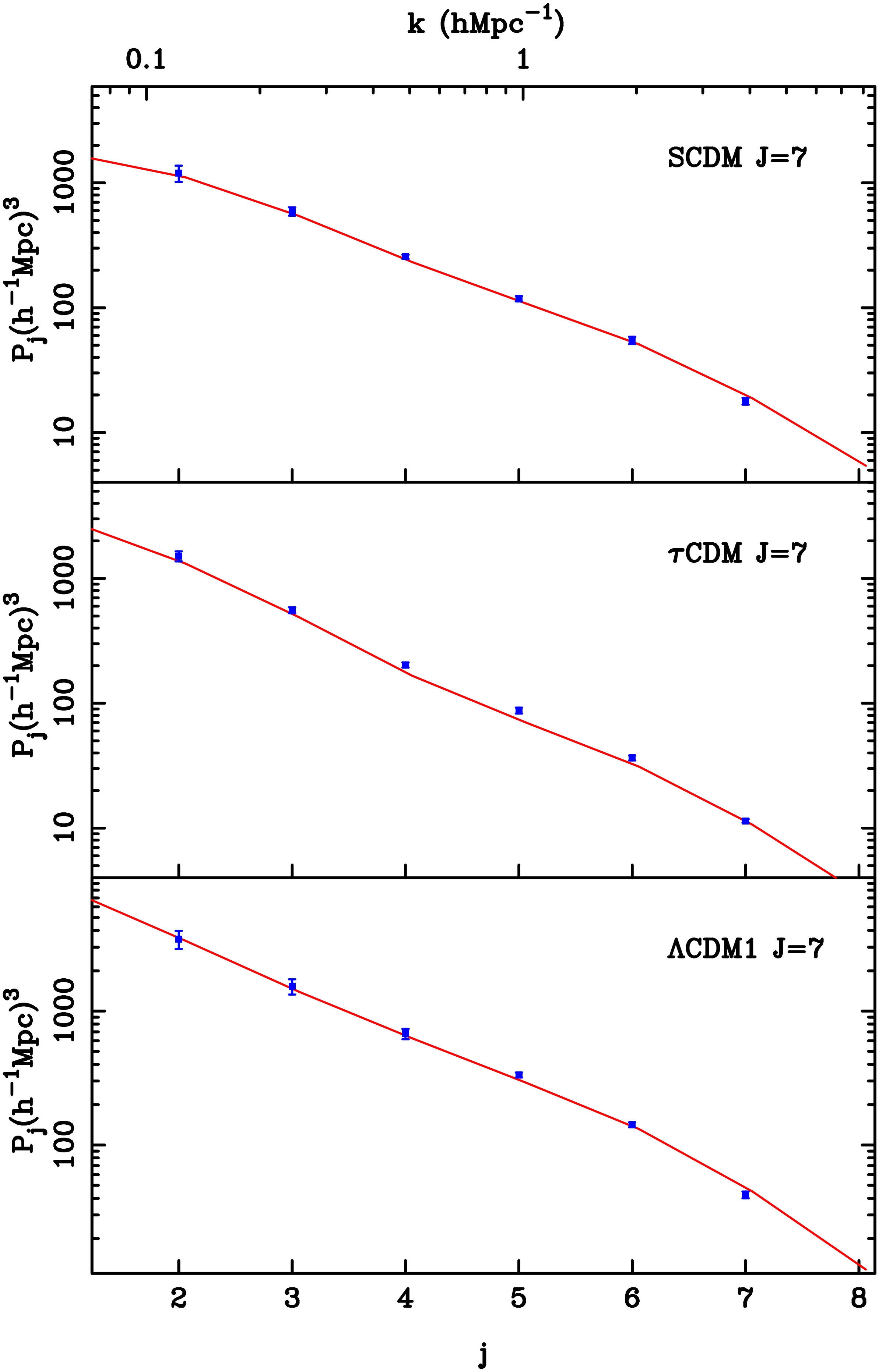
k (hMpc^{-1})
0.1
1
SCDM J=7
τCDM J=7
ΛCDM1 J=7
$P_j(h^{-1}Mpc)^3$
1000
100
10
2
3
4
5
6
7
8
j

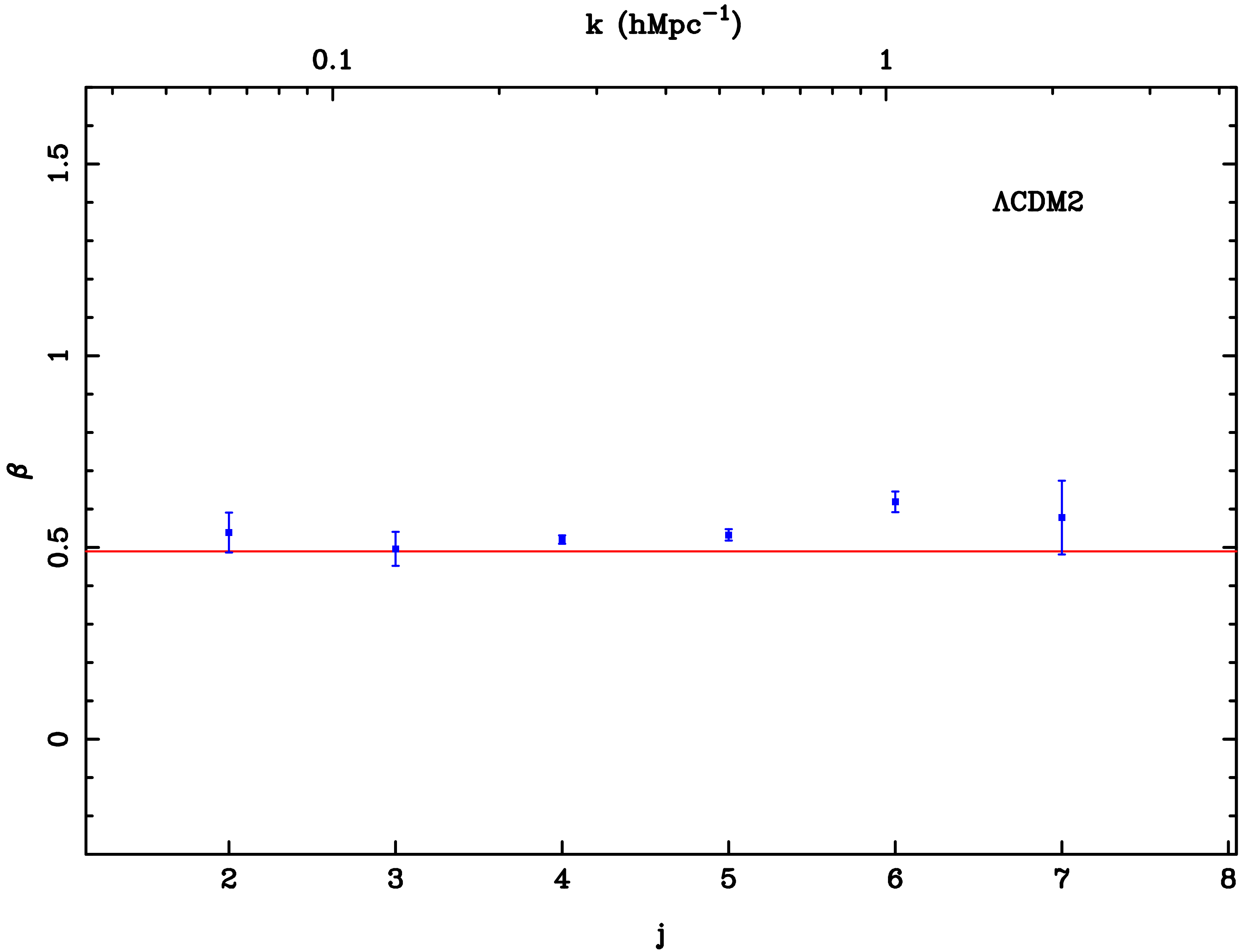
k (hMpc^{-1})
0.1
1
ΛCDM2
β
1.5
1
0.5
0
2
3
4
5
6
7
8
j

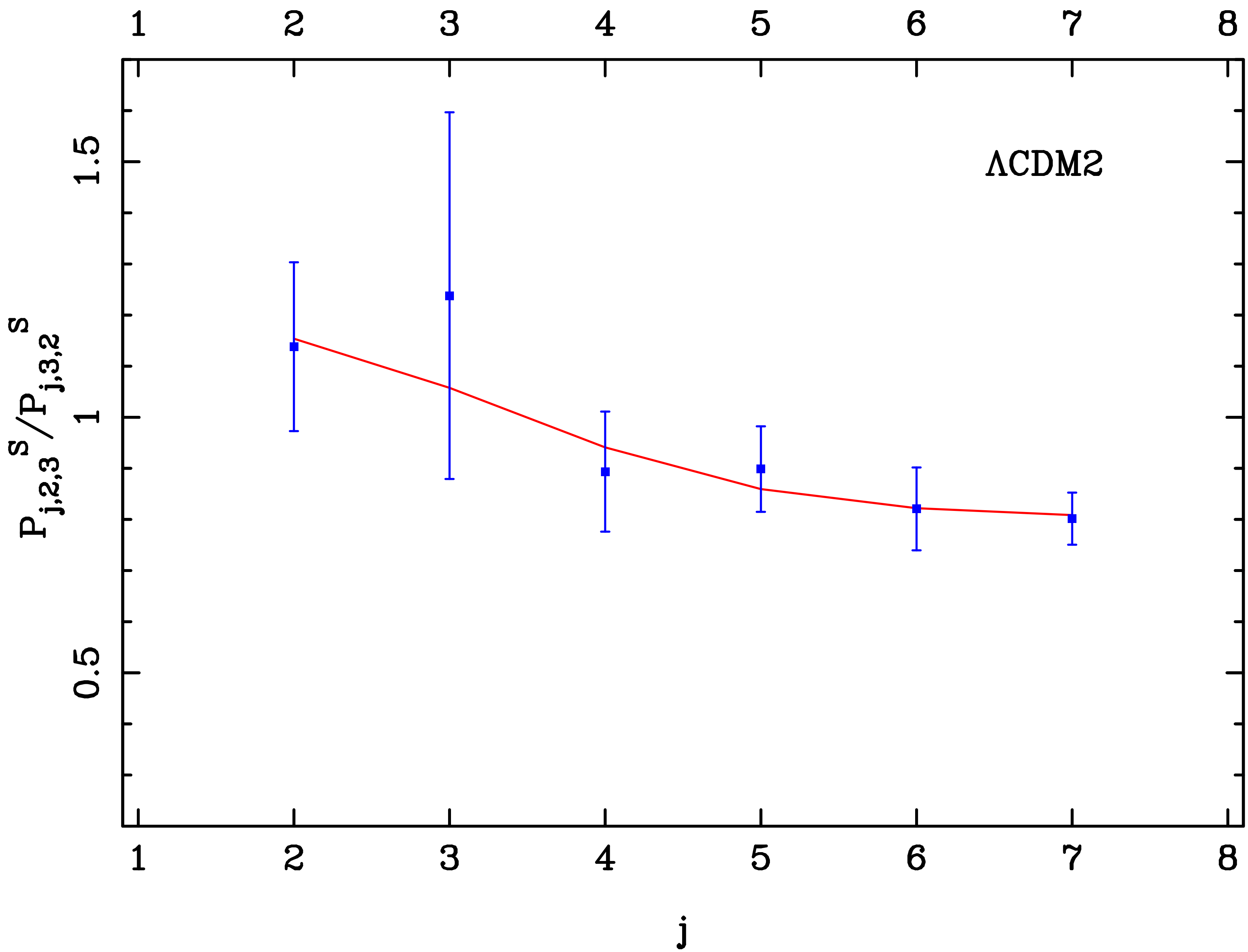

ΛCDM2
$P_{j,2,3}^{S}/P_{j,3,2}^{S}$
j
1
2
3
4
5
6
7
8
0.5
1
1.5

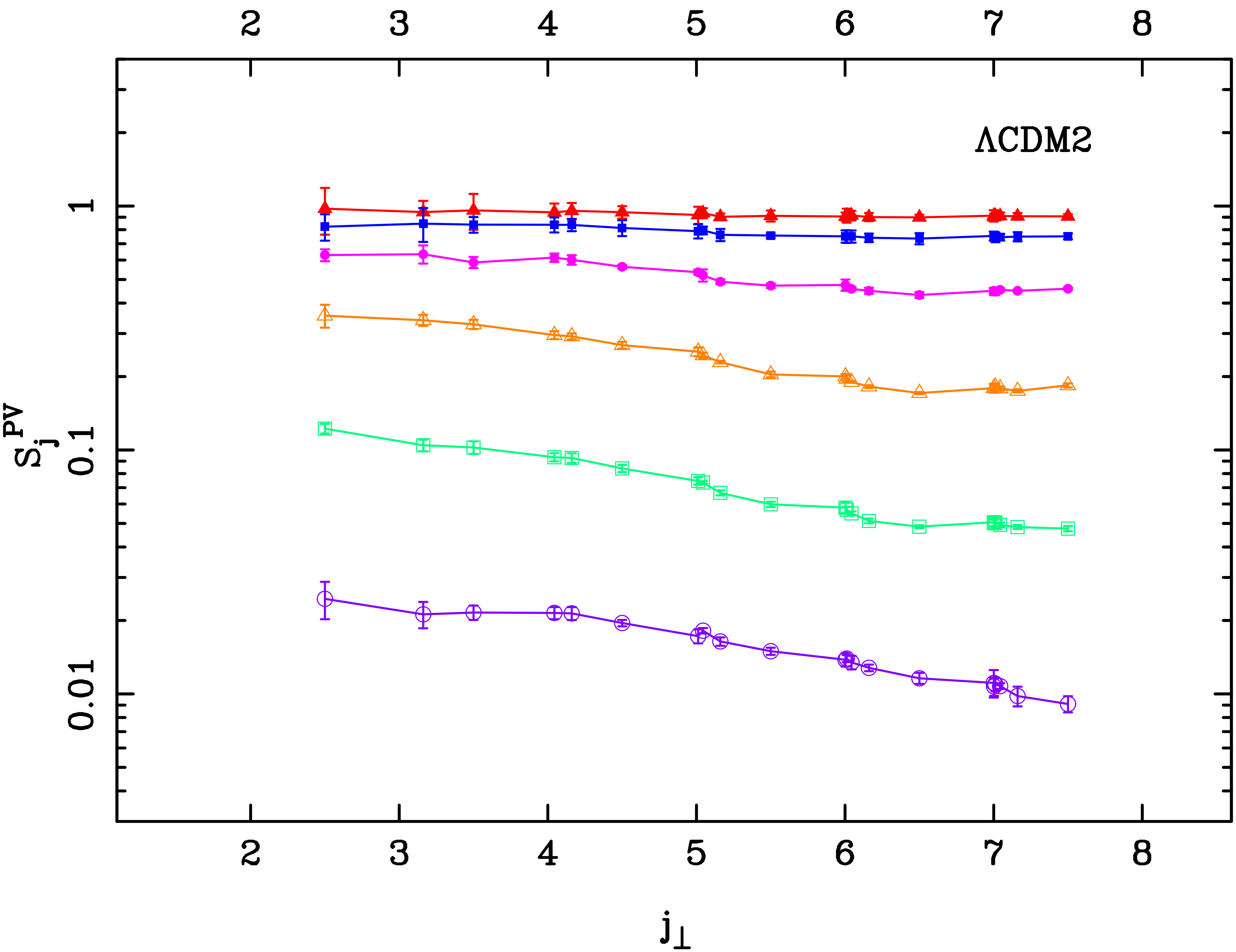

ΛCDM2
1
0.1
0.01
2
3
4
5
6
7
8
S_j^{PV}
$j_\perp$

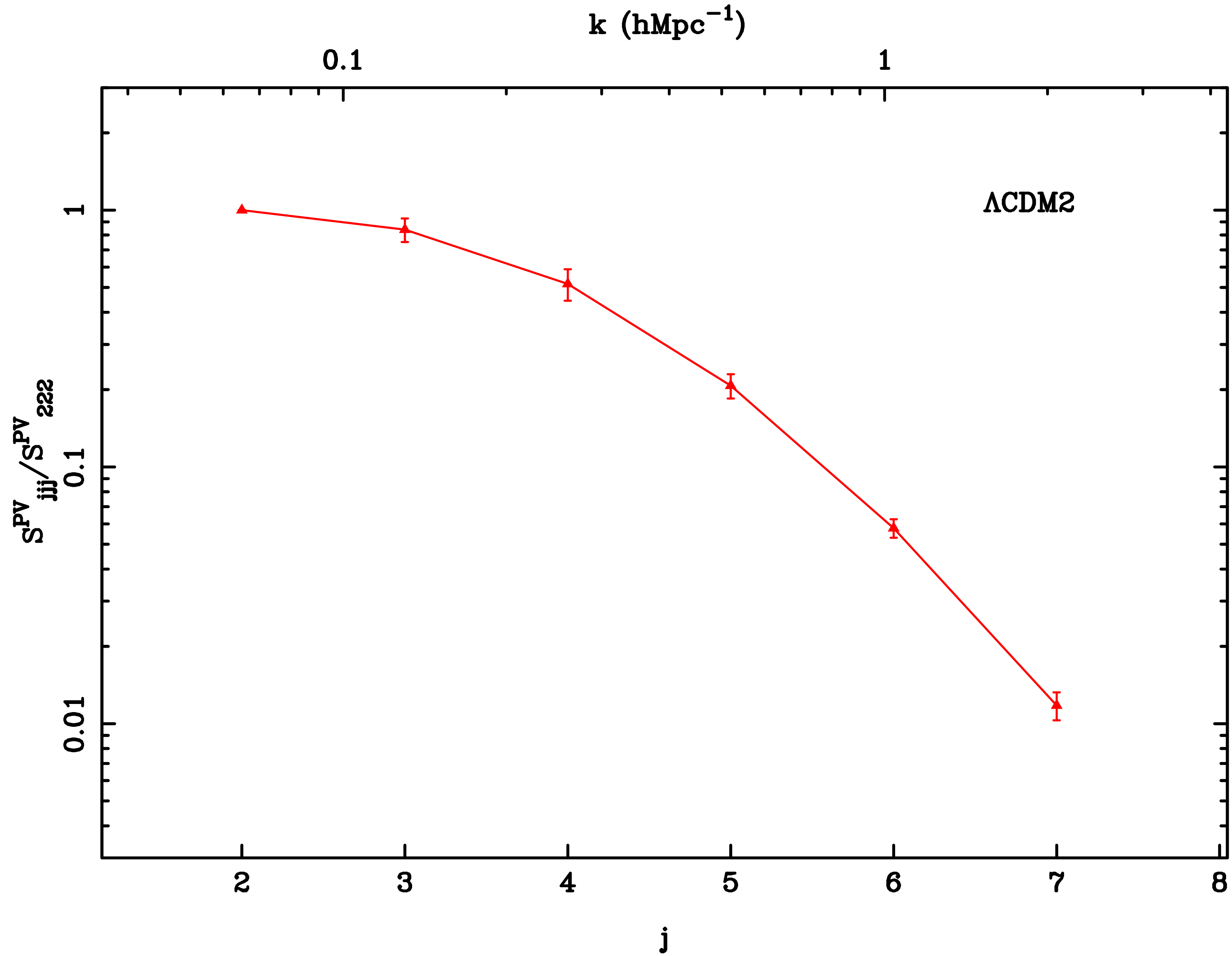

k (hMpc^{-1})
0.1
1
ΛCDM2
$S^{PV}_{jjj}/S^{PV}_{222}$
1
0.1
0.01
2
3
4
5
6
7
8
j

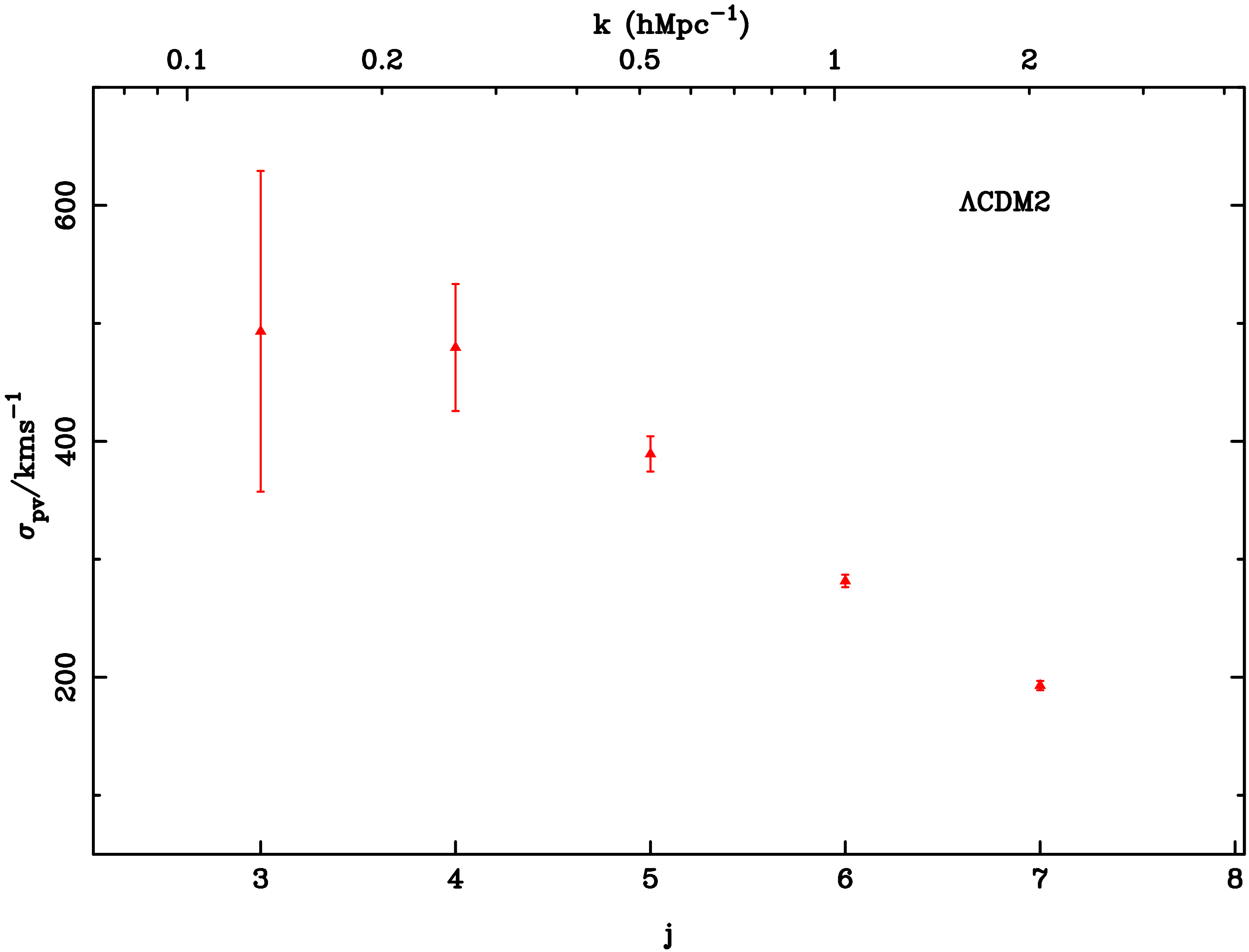
k (hMpc^{-1})
0.1
0.2
0.5
1
2
ΛCDM2
σ_{pv}/kms^{-1}
600
400
200
3
4
5
6
7
8
j

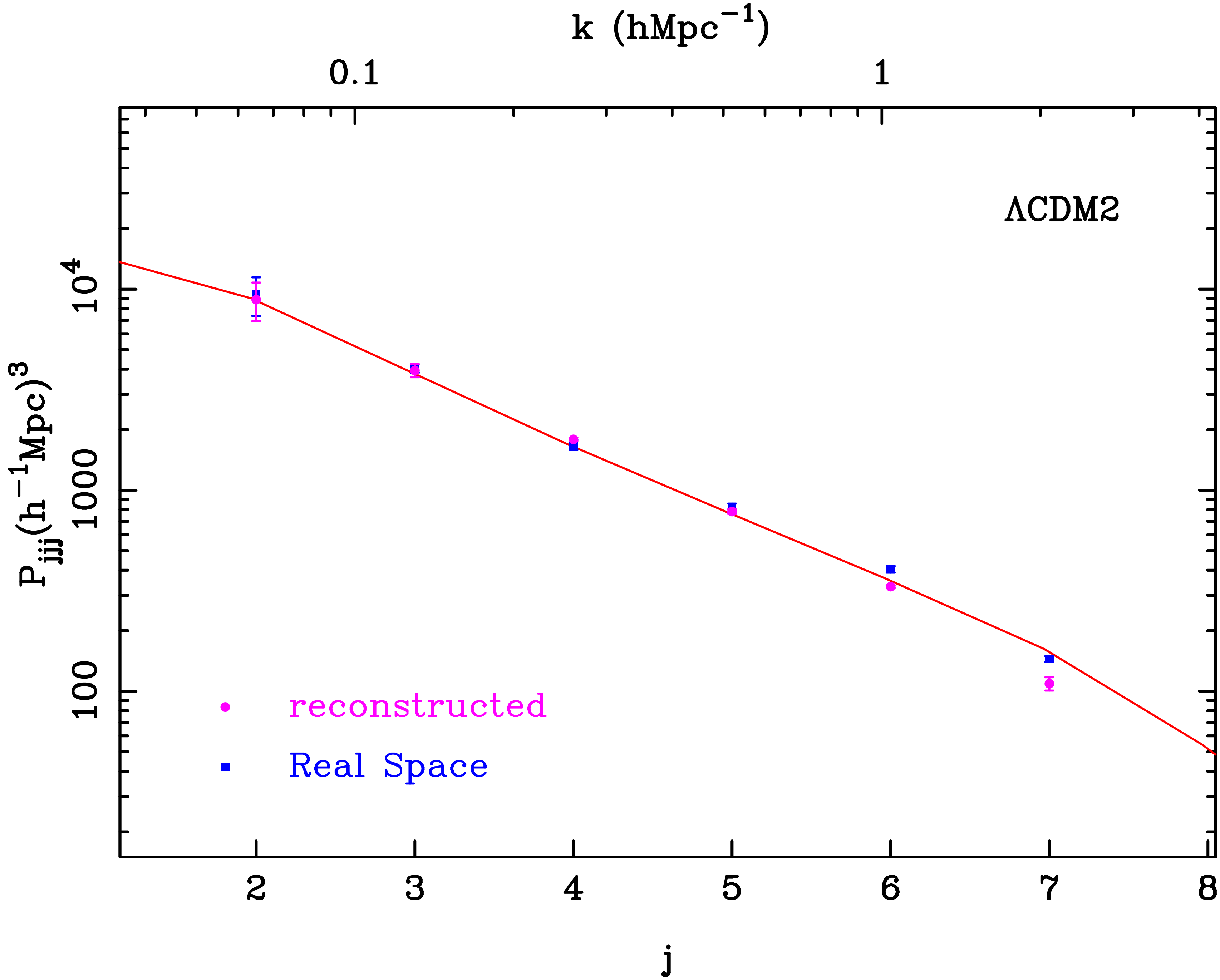
k (hMpc^{-1})
0.1
1
ΛCDM2
10^4
1000
100
$P_{jjj}(h^{-1}Mpc)^3$
reconstructed
Real Space
2
3
4
5
6
7
8
j